Applied Surface Science 257 (2011) 10089–10095

Contents lists available at ScienceDirect

Applied Surface Science

journal homepage: www.elsevier.com/locate/apsusc

Surface characterization of copper, zinc and brass in contact with tap water inhibited with phosphate ions

L. Yohai [a], W.H. Schreiner [b], M. Vázquez [a,*], M.B. Valcarce [a]

[a] División Corrosión, INTEMA, Facultad de Ingeniería, UNMdP, Juan B. Justo 4302 - B7608FDQ Mar del Plata, Argentina
[b] Laboratório de Superfícies e Interfases, Departamento de Física, Universidade Federal do Paraná, 81531-990 Curitiba, PR, Brazil

ARTICLE INFO

Article history:
Received 24 February 2011
Received in revised form 14 June 2011
Accepted 1 July 2011
Available online 7 July 2011

Keywords:
Passive film
Copper
Zinc
Brass
Tap water

ABSTRACT

The composition of the surface layers has been investigated on copper, zinc and brass in contact with moderately hard, highly carbonated and chloride rich artificial tap water (ATW). Cyclic voltammetry, reflectance spectroscopy, X-ray diffraction, Raman spectroscopy and X-ray photoelectron spectroscopy have been used to identify the changes in composition that result from the incorporation of sodium orthophosphate to ATW. The results showed that when PO_4^{3-} is added, the film changes its composition and it also becomes thinner, denser and more compact. On copper, the presence of CuO in the passive film can be correlated to the improvement in the corrosion behavior in the presence of phosphate ions. In the case of brass, the development of a thinner, compact and less porous $Zn_3(PO_4)_2$ layer hinders Cu(I) dissolution. A mechanism explaining the effect of this inhibitor is proposed, which accounts for the experimental results.

1. Introduction

Mar del Plata is a coastal, Argentine city (lat. S:3756 – long. W:5735), where the drinkable water comes only from underground resources. This water is moderately hard and highly carbonated. Due to the marine intrusion of the coastal aquifers, the chloride ions content is relatively high (not less than 100 mg l^{-1}). Argentine food-grade norms fix the upper limit for chloride ions content in 350 mg l^{-1} for drinkable water [1].

Copper and copper alloys are materials broadly used in Mar del Plata drinking distribution systems in valves, heat exchangers, pumps, heating components, plumbing fittings and plumbing fixtures. Aluminum brass is a copper alloy that incorporates zinc as alloying element, so that the mechanical properties of these alloys improve and the cost reduces. Furthermore, the addition of small amounts of aluminum to brass increases the resistance to corrosion in aqueous medium [2].

When an electrolyte allows the development of a compact oxide layer on copper or copper alloys, the metallic surface is protected against general corrosion. However, under these conditions pitting corrosion could be a serious risk when chloride ions are present. In slightly alkaline solutions, brasses present lower pitting resistance than copper due to the incorporation of ZnO in the passive layer [3–6].

Sodium orthophosphate is used as corrosion inhibitor in tap water because in low concentrations it is innocuous for human consumption and has no negative impact on the environment [7]. This corrosion inhibitor acts by minimizing copper dissolution [8–13] and by decreasing the susceptibility to localized corrosion [14,15]. The action mechanism of this inhibitor is not clearly understood but it has been suggested that it reduces the copper solubility forming a cupric phosphate layer on copper [8,16]. Also, Feng et al., found a synergistic inhibitory effect of tripolyphosphate compounds on copper when zinc ions are present in tap water [17]. In addition, when phosphate ions are present in high concentrations, a delay in the onset of the anodic dissolution process on brass has been attributed to the development of a zinc phosphate layer [18,19].

In previous work it has been demonstrated that the corrosion behavior of copper and brass, when they are in contact with a solution that simulates Mar del Plata drinkable water, improves in the presence of phosphate ions [20,21]. A decrease in the copper cuprosolvency together with an increment in the pitting resistances, have been related to changes in the passive films on both materials. These changes have been analyzed using in situ techniques. The results show that when PO_4^{3-} is added as corrosion inhibitor, the film becomes thinner, denser and more compact, changing its composition. In the case of copper, a mechanism has been proposed to explain the increment in the copper corrosion resistance,

* Corresponding author. Tel.: +54 223 481 6600; fax: +54 223 481 0046.
E-mail address: mvazquez@fi.mdp.edu.ar (M. Vázquez).

0169-4332/$ – see front matter © 2011 Elsevier B.V. All rights reserved.
doi:10.1016/j.apsusc.2011.07.002

where the presence of CuO in the passive layer plays a key role [20]. However, in the case of brass, previous results [21] were not enough to establish the composition of the passive film after PO_4^{3-} addition.

In this work, a solution that simulates moderately hard, highly carbonated and chloride rich drinkable water is used. This investigation presents an exhaustive study to evaluate the influence of zinc as alloying element on the corrosion resistance of brass when phosphate ions are present. Therefore, a comparative study of the surface oxide films naturally formed on copper, zinc and brass in contact with drinkable water containing phosphate ions is presented.

2. Materials and methods

2.1. Electrodes preparation

The electrodes were constructed using disc samples of spectroscopy grade copper (99.99%) and aluminum brass UNS 68700 (Cu 76%, Zn 22.18%, Al 1,8% and other impurities 0.02%) provided by LCL Pty Ltd.TM, Australia and with spectroscopy grade zinc (99.99%). To carry out the experiments, metal discs with an appropriated back contact were included in fast curing acrylic resin and mounted on polyvinyl chloride (PVC) holders. The geometrical area exposed was 0.312 cm^2 for copper, 0.785 cm^2 for brass and 0.981 cm^2 for zinc. Samples were abraded to grade 600 with emery paper and then mirror polished with 0.05 μm alumina powder (Type B–Buehler, Lake Bluff, USA). They were finally rinsed gently with distilled water.

2.2. Electrolyte composition

The experiments were carried out using artificial tap water (ATW) simulating the average composition of the drinkable water of an Argentine coastal city. The mineral base composition was $MgSO_4{\cdot}7H_2O$ (40 mg l^{-1}), $MgCl_2{\cdot}6H_2O$ (60 mg l^{-1}), KNO_3 (25 mg l^{-1}), $CaCl_2{\cdot}H_2O$ (110 mg l^{-1}), Na_2CO_3 (470 mg l^{-1}) and $NaNO_3$ (20 mg l^{-1}) in distilled water; the pH was adjusted to 7.6 with 1 mol l^{-1} HCl. The final water conductivity was 1.15 mS cm^{-1}. The final chloride ions concentration determined by potentiometric titration, was 199 mg l^{-1} corresponding to $[Cl^-]$ = 5.6 mmol l^{-1}. The dosage of orthophosphate tested was 10 mg l^{-1} expressed as P, which corresponds to 0.32 mmol l^{-1} $NaH_2PO_4{\cdot}H_2O$, using a 0.05 g ml^{-1} stock solution. This phosphate ions concentration is optimal to avoid generalized corrosion and pitting attack on copper and brass in Mar del Plata drinkable water [20,21].

All the experiments were carried out at room temperature (20 ± 2 °C).

2.3. Electrochemical techniques

The cell and instrumentation employed are standard and have been reported before [20]. All the potentials are indicated against the saturated calomel electrode (SCE).

Copper and brass were pre-reduced at −1.15 V_{SCE} and zinc at −1.65 V_{SCE} during 15 min before each electrochemical experiment. This pre treatment is meant to start from a reproducible, clean surface.

Cyclic voltammograms were recorded after bubbling N_2 during 15 min (deoxygenated solutions). Finally, the potential was scanned at 10 mV s^{-1}, starting at the pre-reduction potential. The potential sweep was reversed at a convenient potential that is indicated where relevant.

After the pre-reduction treatment, passive films were grown during 2 or 192 h at the corrosion potential (E_{corr}) in the electrolyte. Then, the electrodes were immediately transferred to another cell where the oxides were investigated by potentiodynamic reductions in deaerated ATW. The potential was scanned at 10 mV s^{-1} or 1 mV s^{-1}, as indicated in each case. The starting point was the positive potential where the oxide had been grown. The scan ended at −1.15 V_{SCE} on copper and brass, or −1.65 V_{SCE} on zinc.

2.4. UV-visible reflectance spectroscopy

The development of the passive film was also followed in situ, by reflectance spectroscopy. The baseline was recorded polarizing two identical zinc electrodes with a polished surface at −1.65 V_{SCE}. Surface oxides were grown holding the zinc electrode at E_{corr} for 2 h. The spectroelectrochemical measurements were carried out in aerated electrolyte, using a Shimadzu UV 160A double-beam spectrophotometer, which was conveniently modified as described earlier [22,23].

2.5. Ex-situ Raman spectra

Ex-situ Raman spectra were performed on the passive layers on copper, zinc and aluminum brass. The passive layers were grown for 192 h at E_{corr}. After that, the samples were withdrawn, cleaned with de-ionizated water and dried with ethylic alcohol under nitrogen current. Raman spectra were collected at various points (al least five), and were observed to be reproducible.

The Raman measurements were carried out using an Invia Reflex confocal Raman microprobe with Ar^+ laser of 514 nm in backscattering mode, with a laser spot of 10 μm. An exposure time of 50 s and 3 accumulations were used, with 50× objective. The laser power was 25 mW.

2.6. XRD spectroscopy

Samples of copper, zinc and aluminum brass were prepared as described above (Section 2.5) and immediately introduced into X-ray Diffraction (XRD) chamber. XRD was used to identify crystalline phases of copper, zinc and brass. The surfaces of the coupons were analyzed with a PANalytical X'Pert Pro diffractometer, Cu-Kα radiation at 40 kV and 40 mA. Scans were typically over the range of 5°–60° with a speed of 0.02° s^{-1} and grazing incidence of 1°.

The crystallographic data for each phase were taken from the literature and analyzed with X'Pert HighScore software.

2.7. XPS spectroscopy

Samples of copper and aluminum brass were prepared as described above (Section 2.5) and immediately introduced into the XPS chamber. The XPS spectra were performed using an XPS VG Microtech ESCA3000 (MgKα and AlKα radiations) at an operating pressure of 3.10^{-10} mbar. All XPS spectra were acquired with the angle between the analyzer axis and the sample surface normal set at 45°. Survey spectra were recorded for the samples in the 0–1100 eV binding energy range using 1 eV steps and a bandpass of 50 eV (not shown). High resolution scans with 0.1 eV steps and bandpass of 20 eV were conducted over the regions of interest. In every case, surface charging effects were compensated by referencing the binding energy (BE) to the C 1s line of residual carbon set at 284.5 eV BE [24]. The composite XPS bands were resolved using XI SDP32 software, version 3.0.

3. Results

The use of sodium orthophosphate and its effect on the protectiveness of the surface layers on brass in contact with simulated tap water has been investigated earlier [21]. The quality of the passive

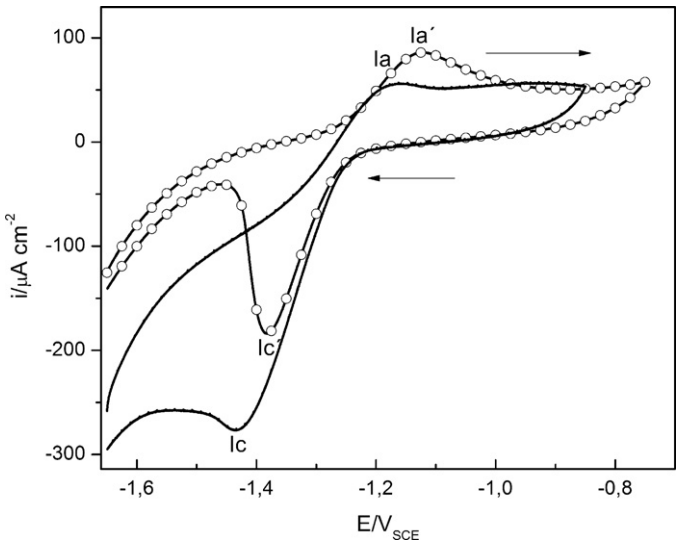

Fig. 1. Cyclic voltammograms of zinc in deaerated ATW (—) and ATW + 10 mg l^{-1} P (–◯–). Scan rate: 10 mV s^{-1}.

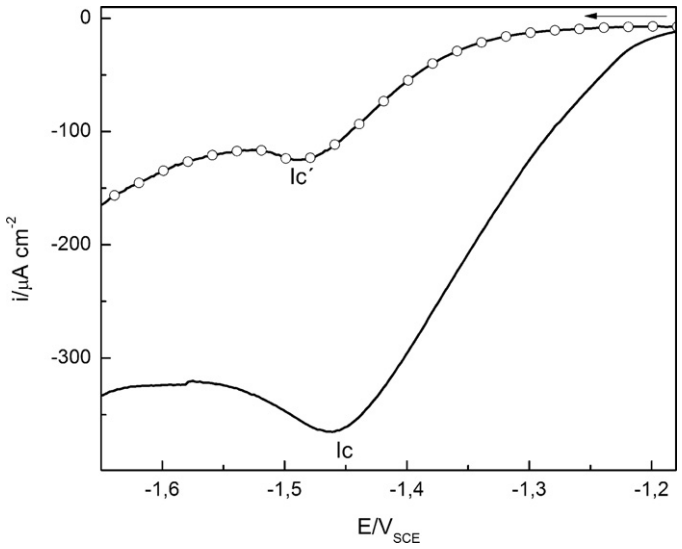

Fig. 2. Potentiodynamic reduction curves for oxides grown on zinc in ATW (—) and ATW +10 mg l^{-1} P (–◯–) after 2 h at E_{corr}, using a scan rate of 10 mV s^{-1}.

film improves, as it becomes less porous, thinner and denser. The incorporation of CuO or Zn(II) compounds to the passive layer could be responsible for this behavior. However, to better understand the role played by the main components in the alloy under the influence of PO_4^{3-} ions, it is necessary to investigate zinc, copper and brass independently.

The voltammograms of pure Zn in ATW and in ATW with inhibitor are presented in Fig. 1. In ATW, oxide growth starts at potentials positive to −1.3 V_{SCE}. There is a small hump (Ia) at −1.15 V_{SCE} followed by a passive region. The electrode presents localized corrosion at potentials positive to −0.81 V_{SCE}. The corresponding cathodic peak (Ic) at −1.4 V_{SCE} can be attributed to Zn(II) oxo-hydroxide reduction [25,26]. In the presence of 10 mg l^{-1} P an anodic peak I′a is observed at −1.13 V_{SCE} while the corresponding cathodic peak is observed at −1.38 V_{SCE} (I′c). The charge of the cathodic peak markedly decreases when the inhibitor is present. Localized attack is now observed at potentials higher than −0.75 V_{SCE}. The voltammograms of copper and brass in the same conditions have been shown before [21].

Fig. 2 shows the potentiodynamic reduction of the layer grown on zinc during 2 h at the E_{corr} in ATW and in ATW with 10 mg l^{-1} P, using a scan rate of 10 mV s^{-1}. E_{corr} stabilizes at −1.04 ± 0.02 and −0.91 ± 0.03 V_{SCE} without and with the inhibitor present in solution, respectively. In both electrolytes, the features observed in the cyclic voltammogram remain: one cathodic peak associated to Zn(II) oxo-hydroxide reduction. When the inhibitor is added, the reduction charge decreases, but no new peak appears associated to $Zn_3(PO_4)_2$ reduction. This might be due to the higher stability of $Zn_3(PO_4)_2$ (pK = 32) compared to ZnO or $Zn(OH)_2$ (pK = 16.7) [19]. Also, Zn(II) reduction from $Zn_3(PO_4)_2$ may not be kinetically favored within the range of potentials applied [17].

Differential reflectance spectroscopy combines optics and electrochemistry, and can be used to follow in situ composition, as thin corrosion films forms. The light beam penetrates between 50 and 100 atomic layers in a semi-transparent solid. So, this technique is useful to identify changes in the surface of the films [27]. Fig. 3 presents reflectance spectra typical of zinc electrodes held at E_{corr} in ATW for 2 h. In both electrolytes, there is a peak at 260 nm that can be ascribed to Zn(II) oxo-hydroxides [5,25,28]. The information on how to distinguish the peaks of Zn(II) phosphates from those of other compounds, such as oxides, is not readily available in the bibliography. When 10 mg l^{-1} P are present, the much lower intensity of the absorption bands, together with the smaller charge associated to the oxides reduction (Figs. 2 and 3), can be correlated to the development of a thinner layer in the presence of inhibitor. This behavior is similar to that found on copper and brass in the presence of PO_4^{3-} ions [20,21].

To complete the surface characterization, ex-situ techniques were used to compare the effect of PO_4^{3-} ions on copper, zinc and brass. To enable the development of a thicker passive layer these films were grown to E_{corr} for longer times.

Fig. 4 shows the potentiodynamic reduction of the layer grown on copper, zinc and brass during 192 h at the E_{corr} in ATW with 10 mg l^{-1} P. When using longer ageing times, slower scan rates (1 mV s^{-1}) are necessary to reduce the surface films. In the case of copper, the cathodic peak at −0.58 V_{SCE} can be associated to CuO reducing to Cu_2O [20]. The second peak at −0.72 V_{SCE} can be associated to Cu_2O reducing to Cu. In the case of zinc, only a hump at −1.5 V could be observed, in agreement with the results presented in Fig. 2. As for brass, one broad peak was observed at −0.74 V_{SCE}, most likely related to the reduction of Cu_2O [21]. No peak associated to the reduction of Zn(II) oxide-hydroxides could be observed, since hydrogen evolution starts at potentials negative to −1.2 V [21].

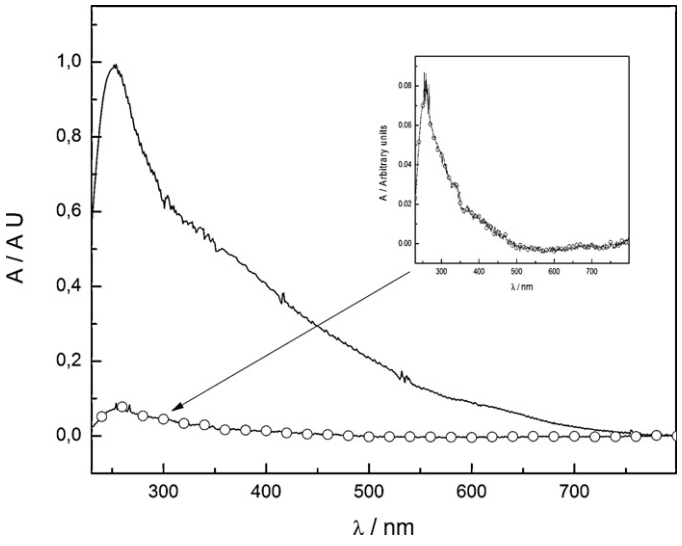

Fig. 3. Reflectance spectra for oxides grown on zinc in ATW (—) and ATW + 10 mg l^{-1} P (–◯–) after 2 h at E_{corr}.

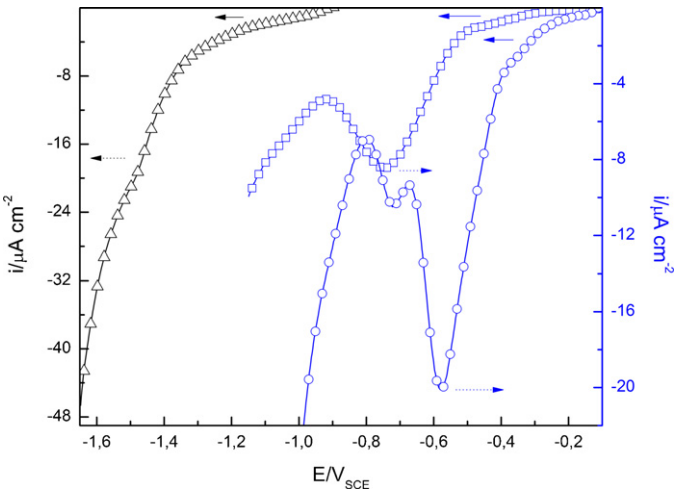

Fig. 4. Potentiodynamic reduction curves for oxides grown on copper (–○–), brass (–□–) and zinc (–△–) after 192 h at E_{corr} in ATW +10 mg l^{-1}P using a scan rate of 1 mV s^{-1}. Scan starts at growth potential.

Raman spectroscopy provides direct information on the bonding, composition and stoichiometry of both crystalline and amorphous surface compounds on metals at atmospheric pressures [29]. Ex-situ Raman spectra of the passive layers grown on copper in ATW and ATW with inhibitor after 192 h at E_{corr} are presented in Fig. 5. In ATW, narrow and intense bands at 150 and 220 cm^{-1} together with a broad feature in the frequency range from 300 and 700 cm^{-1} show that the oxide layer is mainly composed by Cu_2O (*) [30,31]. The identification of CuO by this technique is not possible because Raman scattering from CuO is much weaker than that from Cu_2O and the main peak in the CuO spectrum (♦) lies too close to one of the most intense Cu_2O peaks (*). However, when the inhibitor is added, a decrease of the Raman peak intensity is evident. This fact could be associated with the presence of a Cu_2O and CuO on the surface film, because the scattering from Cu_2O, diluted by CuO, has been reported to be much weaker than that from pure Cu_2O [30].

Ex-situ Raman spectra for passive layers grown on zinc during 192 h at the E_{corr} are presented in Fig. 6. In ATW, the surface layer on Zn shows bands at 380 and 1080 cm^{-1} characteristics of $ZnCO_3$ (□) [32,33] and an increment in the intensity around 140 cm^{-1}, together with bands at 430 and 570 cm^{-1} which are characteristic of ZnO (◊) [33,34]. When the inhibitor is added, the incorporation of PO_4^{3-} ions as $Zn_3(PO_4)_2$ to the passive layer on zinc is evidenced by the intense band that appears at 960 cm^{-1} (●) [32,35,36] together with weak bands at 430 and 570 cm^{-1} [32,35]. The most intense band can be ascribed to the symmetric stretching mode (ν_1) of PO_4^{3-} ions [34,36].

Ex-situ Raman spectra of the passive layers grown on brass for 192 h at E_{corr} are presented in Fig. 7. In ATW, the surface layer on brass is composed of Cu_2O and ZnO. This is supported by the narrow peak at 150 cm^{-1} characteristic of Cu_2O (*), which is overlapped with the band due to ZnO (◊). At 570 cm^{-1} another band of ZnO (◊) is also evident. When the inhibitor is added, the spectrum is flattened as shown in Fig. 7. A decrease in the ZnO and/or Cu_2O participation in the passive film could be associated to this behavior. In addition, the incorporation of PO_4^{3-} ions as $Zn_3(PO_4)_2$ to the passive layer on brass is clear, as shown by the band that appears at 960 cm^{-1} (●).

The XRD spectra of copper, zinc and brass held 192 h in ATW + 10 mg l^{-1} P at the E_{corr} are presented in Fig. 8. The XRD spectrum of copper displays only peaks at 43.3° and 50.4° corresponding to bulk elemental copper (*) (JCPD 1-124). In the case of brass, the two peaks at 42.6° and 49.5° can be related to Cu–Zn phase (♦) (JCPD 25-0322) and other at 38.3° can be related to the presence of an aluminum rich phase (○) [37]. In these spectra, no peaks related to Cu_2O, CuO, $Cu_3(PO_4)_2$ or $Zn_3(PO_4)_2$ can be seen because the passive layers on these metals are very thin (probably thinner than 10 nm) [20,21]. In addition, these compounds may present a poor degree of crystallinity and this technique is limited to crystalline compounds [29,38]. In the case of zinc, XRD spectrum clearly presents peaks at 36.3°, 38.9° and 43.2° related to metallic Zn (◊) (JCPD 4-0831) plus one peak at 32.7°, which could be related to the presence of $ZnCO_3$ (□) (JCPD 3-0774). The incorporation of $Zn_3(PO_4)_2$ (●) to the passive layer is evident with the most intense peaks at 9.6°, 19.3° and 31.4° (JCPD 1-0964).

XPS spectra for passive layers grown on copper and brass in ATW + 10 mg l^{-1} P for 192 h at E_{corr} were recorded. The Cu2p region for both materials is presented in Fig. 9. In the case of Cu_2O, the $Cu2p_{3/2}$ peak is located at a binding energy of 932.2–932.8 eV [17,24,26,39–41], close to the metallic copper signal. With XPS, CuO and $Cu(OH)_2$ can be identified and distinguished from one another,

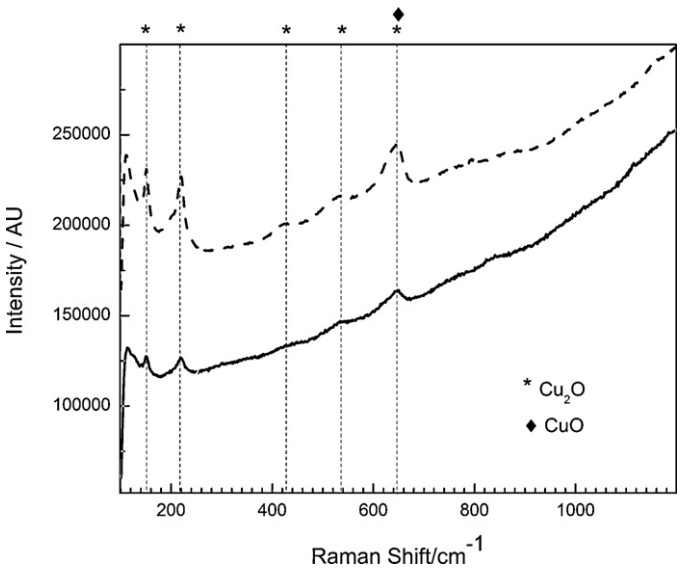

Fig. 5. Ex-situ Raman spectra for passive layers grown on copper in ATW (– –) and ATW + 10 mg l^{-1} P (—) for 192 h at E_{corr}.

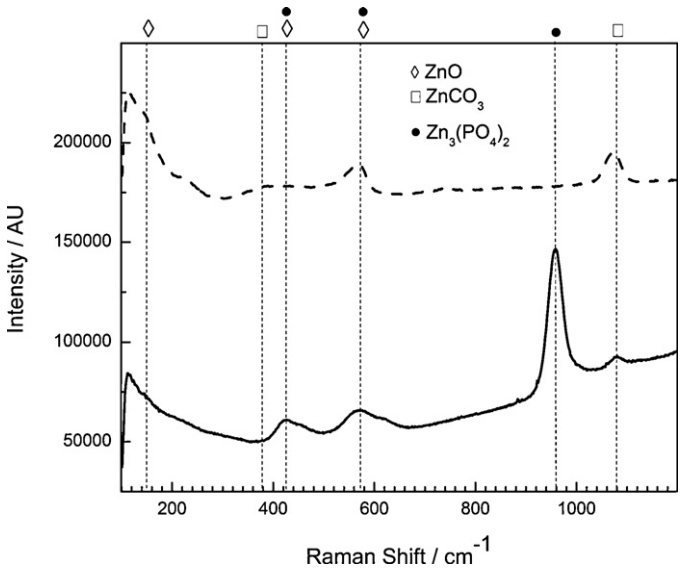

Fig. 6. Ex-situ Raman spectra for passive layers grown on zinc in ATW (– –) and ATW + 10 mg l^{-1} P (—) for 192 h at E_{corr}.

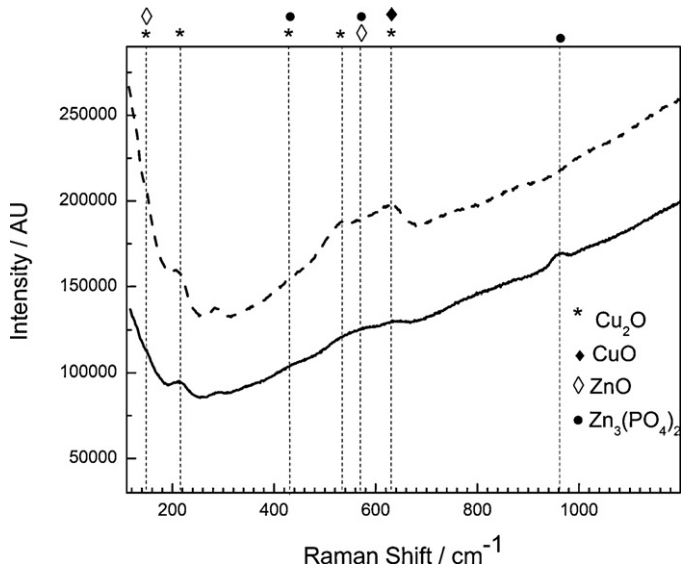

Fig. 7. Ex-situ Raman spectra for passive layers grown on brass in ATW (– –) and ATW + 10 mg l^{-1} P (—) for 192 h at E_{corr}.

because the main $Cu2p_{3/2}$ peak of CuO is around 933.4–934 eV while that of $Cu(OH)_2$ is located at 934.5-935,3 eV [24,26,38,41]. It has also been shown before that Cu(II) compounds present a shake-up peak typical of Cu(II) d^9 ions [26,42]. On the copper spectrum, the shake up peak at 944 eV is present, indicating a high content of Cu(II) compounds in the passive layer. On the other hand, analyzing the brass spectrum, the participation of Cu(II) compounds is not so evident. Table 1 presents the fitting results corresponding to the $Cu2p_{3/2}$ peaks. This fitting was carried out using XI SDP32 software. The peak areas were used to estimate the percentage of the different compounds present in the passive layer. The results presented in Table 1 show that on copper, the Cu(II) compounds contribute in 93% to the global composition while on brass, the

Table 1
Cu2p spectra of copper and brass surface film formed in ATW containing 10 mg l^{-1} P.

	Compound	Position (eV)		Composition (%)
Copper	Cu^0, Cu_2O	932.5	A	7
	CuO	933.4	B	25
	$Cu(OH)_2$	935.2	C	68
Brass	Cu^0, Cu_2O	932.5	A	50
	CuO	933.4	B	37
	$Cu(OH)_2$	935.2	C	13

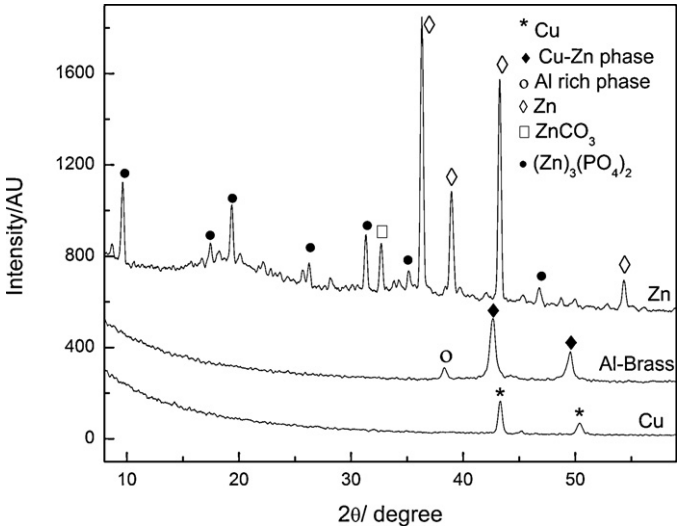

Fig. 8. Grazing XRD spectra of copper, zinc and brass after 192 h in ATW + 10 mg l^{-1} P.

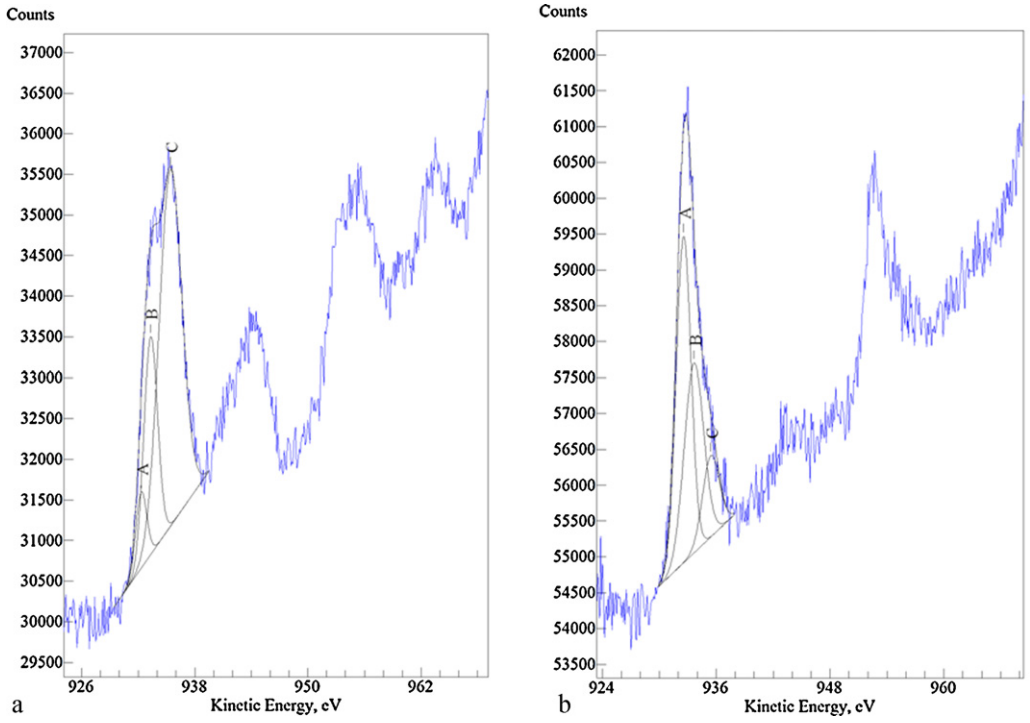

Fig. 9. XPS spectra for passive layers grown on copper (a) and brass (b) in ATW + 10 mg l^{-1} P for 192 h at E_{corr}.

participation of Cu(II) compounds is lower. Also, it has to be considered that the values presented for brass were calculated without taking in account the participation of Zn(II) compounds in the passive layer.

A mechanism that explains the increase in the copper corrosion resistance when phosphate ions are present in ATW has been proposed before [20] and is summarized below. The behavior of copper has been associated to changes in the porosity, thickness and composition of the passive layer.

When passive layers grow on copper the first steps are those shown by reactions (1) and (2) [43,44]:

$$Cu + OH^- \rightarrow Cu(OH)_{ad} + 1e^- \quad (1)$$

$$2Cu(OH)_{ad} \rightarrow Cu_2O + H_2O \quad (2)$$

When PO_4^{3-} ions are present, the solubility of the Cu(I) oxide increases [14,45] resulting in a partial inhibition of the Cu_2O layer formation. Under these conditions CuO can be formed by direct oxidation of Cu^+ ions previously dissolved from the copper surfaces [14,45,46] as shown by reaction (3):

$$Cu^+(aq) + (2-x)H_2O \rightarrow CuO_x(OH)_{2-2x} + 2H^+ + 2e^- \quad (3)$$

Thus, the presence of PO_4^{3-} ions favors the formation of CuO [14,45] which, in turn, is related to the development of a more protective passive layer.

In the case of brass in ATW, an increment of the corrosion resistance when the inhibitor is present has also been established [21]. However, those results were not enough to establish the composition of the passive film and so, only preliminary ideas on the possible mechanism could be outlined. Now, with the complementary results from the surface techniques, a mechanism can be proposed.

When a passive layer grows on brass at the E_{corr}, the first step is the preferential dissolution of Zn from the alloy (reaction (4)), leaving a copper-rich surface [47–49]:

$$Zn \rightarrow Zn^{2+} + 2e^- \quad (4)$$

Subsequently, copper oxide formation begins according the reactions (1) and (2).

As Zn is the most active component in the alloy, Zn^{2+} concentration could be high enough to allow $Zn_3(PO_4)_2$ deposition on the surface [18,19]. The development of a compact passive film of $Zn_3(PO_4)_2$ may reduce Cu(I) dissolution assisted by PO_4^{3-} ions, hindering the deposition of CuO by direct oxidation of Cu(I) from the solution (Eq. (3)).

4. Conclusions

XRD, Raman spectroscopy and XPS have been used to identify the changes in composition of copper, zinc and brass that result from the incorporation of phosphate ions to ATW.

It has been shown before that in the case of brass, a decrease in the copper cuprosolvency, together with an increment in the pitting resistance, may be related to changes in the passive films on copper and brass. The results showed that when PO_4^{3-} is added as corrosion inhibitor the film on copper and brass becomes thinner, denser and more compact. It has now been demonstrated that the films present on zinc are also thinner when phosphates are present. Also, a variety of surface techniques has shown that in all three materials the film changes its composition when in contact with inhibited ATW. All the results are complementary and can be used to establish the mechanism of action for this inhibitor.

On copper, the improvement in the corrosion behavior in the presence of phosphate ions is attributed to the presence of CuO in the passive film and the results confirm the previously proposed mechanism [20].

In the case of brass, the development of a thinner, compact and less porous $Zn_3(PO)_4$ layer hinders Cu(I) dissolution. A mechanism is proposed to support this interpretation, which also explains the improvement on the pitting resistance, found earlier.

Acknowledgements

This work has been supported by the University of Mar del Plata (Grant 15/G225), as well as by the National Research Council (CONICET, PIP0661) and the Agencia Nacional de Promoción Científica y Tecnológica (PICT 6-34112). L. Yohai wishes to thank CIC, Argentina, for her fellowship. The authors are grateful also to Dr. R. Procaccini for his help with the XPS samples.

References

[1] Código Alimentario Argentino, Capítulo XII, artículo 982, Bs. As., Argentina, Ley 18284.
[2] K.M. Ismail, S.S. El-Egamy, M. Abdelfatah, Effects of Zn and Pb as alloying elements on the electrochemical behaviour of brass in borate solutions, J. Appl. Electrochem. 31 (2001) 663–670.
[3] J. Morales, G.T. Fernandez, P. Esparza, S. Gonzalez, R.C. Salvarezza, A.J. Arvia, A comparative study on the passivation and localized corrosion of [alpha], [beta], and [alpha]+[beta] brass in borate buffer solutions containing sodium chloride. I. Electrochemical data, Corros. Sci. 37 (1995) 211.
[4] M.V. Rylkina, Y.I. Kuznetsov, M.V. Kalashnikova, M.A. Eremina, Brass depassivation in neutral chloride media, Protect. Met. 38 (2002) 387–393.
[5] M.B. Valcarce, S.R. de Sanchez, M. Vazquez, Localized attack of copper and brass in tap water: the effect of Pseudomonas, Corros. Sci. 47 (2005) 795–809.
[6] T. Kosec, I. Milosev, B. Pihlar, Benzotriazole as an inhibitor of brass corrosion in chloride solution, Appl. Surf. Sci. 253 (2007) 8863–8873.
[7] M.M. Critchley, N.J. Cromar, N.C. McClure, H.J. Fallowfield, The influence of the chemical composition of drinking water on cuprosolvency by biofilm bacteria, J. Appl. Microbiol. 94 (2003) 501–507.
[8] M. Edwards, L. Hidmi, D. Gladwell, Phosphate inhibition of soluble copper corrosion by-product release, Corros. Sci. 44 (2002) 1057–1071.
[9] S.O. Pehkonen, A. Palit, X. Zhang, Effect of specific water quality parameters on copper corrosion, Corrosion 58 (2002) 156–165.
[10] Y. Zhe, S.O. Pehkonen, Copper corrosion kinetics and mechanisms in the presence of chlorine and orthophosphate, Water Sci. Technol. 49 (2004) 73–81.
[11] S. Li, L. Ni, C. Sun, L. Wang, Influence of organic matter on orthophosphate corrosion inhibition for copper pipe in soft water, Corros. Sci. 46 (2004) 137–145.
[12] N. Souissi, E. Triki, A chemiometric approach for phosphate inhibition of copper corrosion in aqueous media, J. Mater. Sci. 42 (2007) 3259–3265.
[13] N. Souissi, E. Triki, Modelling of phosphate inhibition of copper corrosion in aqueous chloride and sulphate media, Corros. Sci. 50 (2008) 231–241.
[14] M. Drogowska, L. Brossard, H. Menard, Comparative study of copper behaviour in bicarbonate and phosphate aqueous solutions and effect of chloride ions, J. Appl. Electrochem. 24 (1994) 344–349.
[15] D. Lytle, M.N. Nadagouda, A comprehensive investigation of copper pitting corrosion in a drinking water distribution system, Corros. Sci. 52 (2010) 1927–1938.
[16] K. Goh, T. Lim, P. Chui, Evaluation of the effect of dosage, pH and contact time on high-dose phosphate inhibition for copper corrosion control using response surface methodology (RSM), Corros. Sci. (2008) 918–927.
[17] Y. Feng, K.S. Siow, W.K. Teo, K.L. Tan, A.K. Hsieh, Synergistic effects between sodium tripolyphosphate and zinc sulfate in corrosion inhibition of copper in neutral tap water, Corrosion 53 (1997) 546–555.
[18] E.A. Ashour, B.G. Ateya, The effect of phosphates on the susceptibility of alfa-brass to stress corrosion cracking in sodium nitrite, Corros. Sci. 37 (1995) 371–380.
[19] G. Kılınççeker, M. Erbil, The effect of phosphate ions on the electrochemical behaviour of brass in sulphate solutions, Mater. Chem. Phys. 119 (2010) 30–39.
[20] M.B. Valcarce, M. Vázquez, Phosphate ions used as green inhibitor against copper corrosion in tap water, Corros. Sci. 52 (2010) 1413–1420.
[21] L. Yohai, M. Vázquez, M.B. Valcarce, Brass corrosion in tap water distribution systems inhibited by phosphate ions, Corros. Sci. 53 (2011) 1130–1136.
[22] S.R. de Sanchez, L.E.A. Berlouis, D.J. Schiffrin, Difference reflectance spectroscopy of anodic films on copper and copper base alloys, J. Electroanal. Chem. 307 (1991) 73–86.
[23] S. Cere, M. Vazquez, Properties of the passive films present on copper and copper–nickel alloys in slightly alkaline solutions, J. Mater. Sci. Lett. 21 (2002) 493–495.
[24] J.F. Moulder, W.F. Stickle, P.E. Sobol, K.D. Bomben, Handbook of X-ray photoelectron spectroscopy, Physical Electronics Inc., Minnesota, 1995.
[25] M.B. Valcarce, S.R. de Sanchez, M. Vazquez, A comparative analysis of copper and brass surface films in contact with tap water, J. Mater. Sci. 41 (2006) 1999–2007.
[26] I. Milosev, H.H. Strehblow, Electrochemical behaviour of Cu–xZn alloys in borate buffer solution at pH 9.2, J. Electrochem. Soc. 150 (2003) B517–B524.

[27] R.E. Hummel, Differential reflectometry and its application to the study of alloys, Phys. State Sol. A 76 (1983) 12–43.
[28] B.S. Kim, T. Piao, S.N. Hoier, S.M. Park, In situ spectro-electrochemical studies on the oxidation mechanism of brass, Corros. Sci. 37 (1995) 557.
[29] V.S. Sastri, Corrosion Inhibitors, John Wiley and Ltd., West Sussex, England, 1998.
[30] J.C. Hamilton, J.C. Farmer, R.J. Anderson, In situ raman spectroscopy of anodic films formed on copper and silver in sodium hydroxide solution, J. Electrochem. Soc. 133 (1986) 739–745.
[31] G. Niaura, Surface-enhanced Raman spectroscopic observation of two kinds of adsorbed OH^- ions at copper electrode, Electrochim. Acta 45 (2000) 3507–3519.
[32] I.M. Bell, R.J.H. Clark, P.J.G. Christopher, Raman Spectroscopic Library, UCL Chemistry, Faculty of Mathematical and Physical Sciences (MAPS), University College London, 1998.
[33] Z.Q. Tan, C.M. Hansson, Effect of surface condition on initial corrosion of galvanized reinforcing steel embedded in concrete, Corros. Sci. 50 (2008) 2512–2522.
[34] H. Marchebois, S. Joiret, C. Savalla, J. Bernard, S. Touzain, Characterization of zinc-rich powder coatings by EIS and Raman spectroscopy, Surf. Coat. Technol. 157 (2002) 151–161.
[35] A. Tomandl, M. Wolpers, K. Ogle, The alkaline stability of phosphate coatings II: in situ Raman spectroscopy, Corros. Sci. 46 (2004) 997–1011.
[36] R.L. Frost, An infrared and Raman spectroscopic study of natural zinc phosphates, Spectrochim. Acta Part A 60 (2004) 1439–1445.
[37] H.J. Dorantes-Rosales, V.M. López-Hirata, J.L. Méndez-Velázquez, Microstructure characterization of phase transformations in a Zn-22 wt.%Al-2 wt.%Cu alloy by XRD, SEM. TEM and FIM, J. Alloys Compd. 313 (2000) 154–160.
[38] W. Xiao, S. Hong, Z. Tang, S. Seal, J.S. Taylor, Effects of blending on surface characteristics of copper corrosion products in drinking water distribution systems, Corros. Sci. 49 (2007) 449–468.
[39] E. Cano, M.F. López, j. Simancas, J.M. Bastidas, X-ray photoelectron spectroscopy study on the chemical composition of copper tarnish products formed at low humidities, J. Electrochem. Soc. 148 (2001) E26–E30.
[40] T. Ghodselahi, M.A. Vesaghi, A. Shafiekhani, A. Baghizadeh, M. Lameii, XPS study of the Cu@Cu_2O core-shell nanoparticles, Appl. Surf. Sci. 255 (2008) 2730–2734.
[41] Y. Feng, W.K. Teo, K.S. Siow, K.L. Tan, A.K. Hsieh, The corrosion behaviour of copper in neutral tap water. Part I. Corrosion mechanism, Corros. Sci. 38 (1996) 369–385.
[42] M.C. Biesinger, B.P. Payne, B.R. Hart, A.P. Grosvenor, S. McIntryre, L.W.M. Lau, R.S.C. Smart, Quantitative chemical state XPS analysis of first row transition metals, oxides and hydroxides, J. Phys.: Conf. Ser. 100 (2008), 012025.
[43] A.M.C. Luna, S.L. Marchiano, A.J. Arvia, Electrochemical formation and cathodic dissolution of a thin cuprous oxide film on copper in alkaline aqueous solution, J. Electroanal. Chem. 59 (1975) 335–338.
[44] S.M. Wilhelm, Y. Tanizawa, C.Y. Liu, N. Hackerman, A photo-electrochemical investigation of semiconducting oxide films on copper, Corros. Sci. 22 (1982) 791–805.
[45] M. Drogowska, L. Brossard, H. Ménard, Effects of phosphate ions on copper dissolution and passivation, J. Electrochem. Soc. 139 (1992) 2787–2793.
[46] R. Babic, M. Metikos-Hukovic, A. Jukie, A study of copper passivity by electrochemical Impedance spectroscopy, J. Electrochem. Soc. 148 (2001) B146–B151.
[47] H.W. Pickering, Characteristic features of alloy polarization curves, Corros. Sci. 23 (1983) 1107–1109.
[48] R.S. Scherebler, C.H. Gomez, J.I. Gardiazabal, Potentiodynamic behaviour of α brass in 1 M Na_2SO_4 solution, Corrosion 43 (1987).
[49] L. Burzynska, Comparison of the spontaneous and anodic processes during dissolution of brass, Corros. Sci. 43 (2001) 1053–1069.